International Journal of Mechanical Sciences 241 (2023) 107927

Contents lists available at ScienceDirect

International Journal of Mechanical Sciences

journal homepage: www.elsevier.com/locate/ijmecsci

Convective heat transfer modelling in dry-running polymer spur gears

Victor Roda-Casanova *, Francisco Sanchez-Marin, Raul Martinez-Cuenca

Department of Mechanical Engineering and Construction, Universitat Jaume I, Spain

ARTICLE INFO

Keywords:
Heat transfer coefficient
Polymer gears
Computational fluid dynamics
Heat convection

ABSTRACT

Heat convection is an important phenomenon in the process of cooling polymer spur gears running in dry conditions, which ultimately affects the strength of the gears. In order to gain some insight into this phenomenon, a numerical heat convection model for polymer spur gears is proposed in this work, which is based on a detailed CFD simulation of the gears in operating conditions and it allows us to investigate the heat convection through their external surfaces.

The performance of this numerical model is illustrated with several examples, in which a parametric study has been conducted to observe the variation of the heat transfer coefficients with the face width and the angular speed of the gears. The results obtained from this parametric study are compared to those obtained from a representative classical heat convection model, observing that the relative differences between them in terms of heat transfer coefficients can be as high as 125%.

Finally, a new optimized heat convection model for polymer spur gears running in dry conditions is proposed, in which the convective heat transfer coefficients for the external surfaces of the gears are calculated from empirical equations based on the Newton's law of cooling. This optimized model has lower computational cost than the numerical one, while it provides an important increase of the accuracy of the classical heat convection models, reducing the maximum relative differences to 10%.

1. Introduction

One of the limitations of using polymer gears for power transmission is their sensitivity to changes in their temperature. Increases in temperature diminish the mechanical properties of the polymer gears, because they reduce the elastic modulus of the polymer material, as well as their bending and rolling contact fatigue strength [1]. This is especially problematic, since in these transmissions there are several effects that favour temperature rises in the gears. On the one hand, these transmissions are usually operated without any lubricant, so an important amount of frictional heat is generated during the meshing of the gears [2]. On the other hand, the lack of lubricant reduces the convective cooling capabilities of the transmission. These facts, combined with the low thermal conductivity of the material, accentuate the increments in temperature. For these reasons, predicting the temperature of the gears in operating conditions is an important step during the process of designing polymer gear transmissions, and several analytical and numerical methods have been developed for such a purpose.

The most relevant analytical methods to determine the bulk temperature of polymer gears are those derived by Hachmann [3,4], Takanashi [5] and Mao [6]. The analytical determination of the flash temperature is usually performed using the method proposed by Blok [7]. These methods have the advantage of being fast and easy to implement, but they have several limitations imposed by the hypotheses of the underlying theory [8]. Let us note that other analytical methods, such as the differential transform method [9], the adomian decomposition method [10,11] or even the optimal homotopy asymptotic method [12], could be interesting for the resolution of temperature fields in polymer gear transmissions, but to date they have not been used for this purpose.

Some of the limitations of the analytical methods can be overcome by using numerical methods. Although some exceptions can be found in the literature [13–15], numerical methods are mostly based on finite element thermal analyses of the gears, where the frictional and the hysteretic heat generated during the meshing of the gears are introduced as thermal loads on the finite element model of a gear. All the heat transfer mechanisms (conduction, convection and radiation) can be considered in these analyses, although radiation is usually disregarded because its effect is negligible compared to the effect of the other two mechanisms. In these thermal finite element analyses, convection is considered through surface film conditions, which are a kind of boundary conditions that are applied to the external surfaces of the gear.

The specification of these surface film conditions requires the calculation of the heat transfer coefficients (HTC) associated to each of them.

* Corresponding author.
E-mail address: vroda@uji.es (V. Roda-Casanova).

https://doi.org/10.1016/j.ijmecsci.2022.107927
Received 6 August 2022; Received in revised form 25 October 2022; Accepted 11 November 2022
Available online 16 November 2022

Nomenclature

Subscripts

1	Relative to the pinion
2	Relative to the wheel
air	Relative to the surrounding air
i	Relative to node i
j	Relative to surface j
k	Relative to analysis frame k

Symbols

b	Face width
cp	Specific heat
d	Reference diameter
d_a	Tip diameter
d_f	Root diameter
H	Enthalpy
h	Instantaneous local heat transfer coefficient
$\hat{h}$	Instantaneous global heat transfer coefficient, IG-HTC
$\hat{h}'$	Time-averaged global heat transfer coefficient, AG-HTC
L_c	Characteristic length of a surface
m	Module
Nu	Nusselt number
p	Pressure
Pr	Prandtl number
Q	Thermal power
q	Heat flux
Re	Reynolds number
S	Source term
s_a	Transverse tooth thickness at the tip circle
s_t	Transverse tooth thickness at the reference circle
T	Temperature
t	Time
v	Speed
v	Velocity vector
z	Number of teeth
α	Pressure angle
δ	Kronecker delta
γ	Thermal expansion
λ	Thermal conductivity
μ	Dynamic viscosity
ν	Kinematic viscosity
ω	Angular speed
ρ	Density
$\boldsymbol{\tau}$	Stress tensor

These HTCs are constants that relate the amount of convective heat flux to the temperature difference between the gears and the surrounding air, and their calculation constitutes one of the important challenges during the preparation of these finite element models. Bearing this in mind, a *heat convection model* will be defined as the set of surface film conditions specified on the gears and the way in which the HTCs are calculated for each of them.

As explained by Handschuh [16], it would be desirable to collect these HTCs from empirical data, but accomplishing this would require a separate and very involved experimental effort. For this reason, in the great majority of the heat convection models found in the literature, these coefficients were determined by considering certain parts of the gear geometries as simple geometric shapes (cylinders, plates, discs, etc.) subjected to typical air flows. From now on we will refer to these models as *classical heat convection models*. A huge variety of different correlations between the gear surfaces and simple geometrical objects can be found in these models, and it is difficult to know which of them provides a better description of the actual physical phenomena.

Early attempts to predict the bulk temperature of the gears using a finite element thermal analysis were made by Patir [17] in 1979, who used a two-dimensional finite element model for this purpose. In that study, Patir considered a metallic gear transmission subjected to jet-cooling, and hence he used a heat convection model in which the HTC for the gear flanks was calculated using the equations proposed by DeWinter [18] and Heijningen [19].

Important advances in the finite element modelling of the thermal behaviour of gear transmissions were made by Handschuh [16,20] during the last decade of the $20th$ century. The same author proposed a method to conduct a three-dimensional finite element thermal analysis of spiral bevel gears, in which the use of a moving heat flux allowed the determination of the steady-state and transient temperature fields over a tooth of a spiral bevel pinion. In these studies, Handschuh defined a heat convection model in which the external boundary of the gear was divided into three surface film conditions: one for the active flanks, one for the gear sides and one for the rest of the gear surfaces (tooth tip, tooth root and coast side). To calculate the HTC for the active flank, this surface was viewed as a plate moving perpendicular to the nominal ambient conditions, and this simplification allowed the use of the equation proposed by Holman [21]. Regarding the calculation of the HTC for the gear sides, Handschuh viewed the gear as a disc rotating in quiescent air, and he used Hartnett's relation [22] to determine the corresponding HTC. Finally, the HTC for the tooth tip, tooth root and coast side were arbitrarily set between the value for an insulated boundary and the value defined for the gear sides.

In 2003, Long [23] developed a steady-state thermal finite element model to determine the operating temperature of oil-lubricated medium-speed metallic gears, which accounts for the effect of oil mist as a cooling medium. In that work, Long considered a heat convection model in which the external boundary of the gear was divided into two surface film conditions: one for the gear flanks and one for the gear sides. As in Patir's work, the HTC for the gear flanks was calculated using the equations proposed by DeWinter [18]. The novelty of this work was that three different equations were considered for the calculation of the HTCs for the gear sides, depending on the type of flow expected alongside these surfaces: laminar [22], transitional [24] or turbulent [25].

A large number of studies have used these heat convection models (or combinations between them) to set up the finite element models to conduct thermal analyses of metallic gear transmissions. To provide some examples, Taburdagitan [26] determined the rise in surface temperature of spur gears with thermo-elastic finite element analyses. Shi [27] used a thermal finite element analysis to study the bulk temperature field and the flash temperature in a locomotive traction gear. Luo and Li [28] studied the influence of several design parameters and operating conditions on the temperature field of gears by means of thermal finite element analyses. Li continued using thermal finite element analyses to perform studies on the unsteady-state temperature field of gear transmissions [29], to analyse the thermal characteristics of spur/helical gear transmissions [30], and to conduct thermal analyses of helical gear transmissions considering misalignment [31].

Similar heat convection models were used to consider the convection phenomenon in the thermal analyses of polymer gear transmissions. Doll [32,33] was one of the first researchers to propose a thermal finite element model to determine the temperature field over polymer gears. He was also a pioneer in considering the heat generated by hysteresis of the gear material in this kind of finite element analyses. In

these works, Doll set up a heat convection model in which the external boundary of the gear was divided into two surface film conditions: one for the tooth flanks and one for the gear sides. In this heat convection model, the HTC for the gear sides was predicted from experimental correlations for the side surface of a disc rotating in quiescent air [34], whereas the HTC for the tooth flanks was predicted from the principle of flow across cylinders [35].

Later on, Fernandes [36] proposed a thermal finite element model to predict the bulk and flash temperatures on polymer gears considering oil-jet lubrication, dip lubrication or non-lubricated conditions. In that work, Fernandes combined the heat convection models proposed by Long [23] and Handschuh [16] to define the convective behaviour of the thermal finite element model. A similar heat convection model was also used by the authors of this work [37,38].

Recently, Černe [39] developed a thermo-mechanical finite element model of polymer spur gears that was experimentally validated using high-speed infrared thermography. In that work, the heat convection model considered three different surface film conditions: one for the tooth flanks, one for the tooth sides and one for the gear sides. The way in which the HTC for each surface film condition is calculated differs from the rest of the works reviewed, and it is explained in detail in Appendix. To the authors' knowledge, this is currently the most advanced model to predict the temperature field on polymer gears.

As can be observed, there is a wide variety of classical heat convection models in the literature, and each of them has a different number of surface film conditions and a different way to calculate the HTCs associated with them. This fact shows us that there is no consensus among researchers on how these correlations between the gear surfaces and simple geometrical objects should be addressed, because the degree of similarity between the HTCs of the simple geometric shapes and the actual gear surfaces has not been tested [16,17,23,32].

To overcome these issues, Wang [40] developed a *numerical heat convection model* based on a Computer Fluid Dynamics (CFD) analysis of the transmission to determine the HTCs for the gear surfaces, considering that the gear is running under oil-jet lubrication conditions. From the perspective of the polymer spur gears running in dry conditions, the main drawback of the numerical model developed by Wang is that it does not take into account the engagement of the gear teeth, which has a significant effect on the air flow and the convection phenomenon in this type of gear transmissions, as pointed out by Mao [6].

Other authors have shown interest in applying CFD simulations to investigate different phenomena in gear transmissions. Concli [41] and Mastrone [42,43] used CFD simulations to analyse the effects of the lubricant in the power losses of a gear transmission. Lu [44] and Liu [45] used CFD simulations to study the thermal behaviour of a gear transmission with splash and injection lubrication, respectively. Renjith [46] and Deshpande [47] used similar approaches to investigate the thermal performance of oil-jet lubricated gear transmissions. Kara [48] studied the turbulent flow around a spur gear pair to predict the load-independent windage power losses. Recently, Ouyang [49] developed a CFD-vibration coupled model to predict cavitation in gear transmissions. However, no other numerical work devoted to studying in depth the convection phenomenon in polymer spur gears running in dry conditions has been found in the literature.

In general, the determination of the HTCs to simulate the convective heat transfer in polymer gears still remains a concern when calculating the temperature field of polymer gears through a thermal finite element analysis. Based on these facts, the objectives of this work are:

i. To propose a *numerical heat convection model* for polymer spur gear transmissions running in dry conditions.
ii. To use this *numerical heat convection model* to investigate the convection phenomenon under different gear geometries and running conditions.
iii. To compare the *numerical heat convection model* with the *classical heat convection models* that are currently used in the thermal analysis of polymer gears.
iv. To propose an *optimized heat convection model* to enhance the simulation of the convective cooling in polymer spur gears running in dry conditions.

2. Convective heat transfer modelling in thermal finite element analyses: statement of the problem and overview of the work

In the thermal finite element analyses of polymer gear transmissions running in dry conditions, convective heat transfer is modelled through surface film conditions that are applied to the external boundary of each gear geometry (i.e. those parts of the gear geometry that are in contact with the surrounding air). For this purpose, the external boundary of the gear geometry is divided into a set of surfaces, in such a way that the heat transfer coefficient can be considered constant along each of them. Then, for each of these surfaces, a Neumann boundary condition is applied in the form:

$$\lambda \cdot \frac{\partial T}{\partial \mathbf{n}} = -h \cdot \left(T_\infty - T\right) \tag{1}$$

where λ is the thermal conductivity of the gear material, T_∞ is the temperature of the environment and h is the convective heat transfer coefficient specified for the surface. Moreover, $\mathbf{n}$ is a unit vector indicating the normal direction at a given point on the surface, and T is the temperature at such a point (unknown). Thus, in the great majority of commercial finite element packages, the surface film condition for a given surface is specified through the heat transfer coefficient and the temperature of the environment. In consequence, one of the major challenges when conducting a thermal finite element analysis of a gear drive is the determination of this coefficient for each surface film condition considered.

The heat transfer coefficient depends on the geometry of the surface, the thermal properties of the surrounding air and the relative motion between this air and the surface under study, and it is calculated as [50]:

$$h = \frac{\lambda_{air}}{L_c} \cdot Nu \tag{2}$$

where λ_{air} is the thermal conductivity of the surrounding air, L_c represents the characteristic length of the observed surface and Nu is the Nusselt number, which is often calculated from the Reynolds number Re and the Prandtl number Pr as:

$$Nu = C_1 \cdot Re^{C_2} \cdot Pr^{C_3} \tag{3}$$

where C_1, C_2 and C_3 are coefficients that need to be adjusted for each surface film condition considered over the gears, either using experimental or theoretical analyses. Here resides the problem of modelling the convective heat dissipation in polymer gears: while these coefficients have been adjusted for simple geometrical objects (cylinders, plates, etc.) subjected to typical airflows, no exhaustive experiments have been conducted to adjust them for the surfaces of a rotating gear [16].

In general, this work is devoted to investigating in depth the convective behaviour of polymer gears running in dry conditions and, in particular, to studying the heat transfer coefficients that should be specified in the external surfaces of the gears in order to reproduce their actual convective behaviour in a thermal finite element analysis. For this purpose, three different heat convection models are considered for the polymer gears:

- The classical heat convection models for polymer gear transmissions [23,36,39], which consist in approximating the external surfaces of the gear to simple geometrical objects, and then using their coefficients to calculate the Nusselt number (Eq. (3)) and the heat transfer coefficient (Eq. (2)) of the gear surfaces (see Appendix).

- A new numerical heat convection model based on a CFD analysis of the gear transmission, which consists in a detailed simulation of the polymer gears in operating conditions (including the effect of the tooth engagement) and the post-processing of the results in order to obtain the heat transfer coefficients of the external surfaces for the gears (see Section 3).
- A new optimized heat convection model, which is based on the use of Eqs. (2) and (3), but with empirically adjusted coefficients to match the results obtained from the CFD analysis for a given set of case studies (see Section 4.3).

3. A CFD heat convection model to investigate the convective behaviour of polymer spur gears

The simulation of fluid flow through CFD techniques has become a tool of primary importance in numerous fields of engineering: nuclear reactor design [51], aerogenerator design [52], wastewater treatment [53,54], winds and air-pollutant dispersion in cities [55] or refrigeration [56] are just some recent examples of its uses. CFD simulations have also been applied to study several aspects related to gear transmissions [41–49], but very few examples can be found in the literature where CFD simulations are used to investigate the convective cooling of polymer gears running in dry conditions [57].

In this section a new numerical heat convection model based on a CFD analysis is proposed to study the convective heat transfer coefficients through the external surfaces of a polymer spur gear running in dry conditions. The following subsections detail the CFD modelling framework, the CFD simulation and the calculation of the heat transfer coefficients from the results of the CFD simulations.

3.1. CFD modelling framework

The CFD model proposed in this work solves the flow surrounding a pair of moving gears based on the so-called unsteady Reynolds-Averaged Navier–Stokes (uRANS) equations. This approach leads to the following set of conservation equations (Eqs. (4)–(6)):

- Mass

$$\frac{\partial \rho_{air}}{\partial t} + \nabla \cdot \left(\rho_{air}\ \mathbf{v}\right) = 0 \tag{4}$$

- Momentum

$$\frac{\partial \left(\rho_{air}\ \mathbf{v}\right)}{\partial t} + \nabla \cdot \left(\rho_{air}\ \mathbf{v} \otimes \mathbf{v}\right) = -\nabla p + \nabla \cdot \boldsymbol{\tau} + \mathbf{S}_M \tag{5}$$

- Total enthalpy

$$\frac{\partial \left(\rho_{air}\ H_{tot}\right)}{\partial t} - \frac{\partial p}{\partial t} + \nabla \cdot \left(\rho_{air}\ \mathbf{v}\ H_{tot}\right) = \nabla \cdot \left(\lambda_{air}\ \nabla T\right) + \nabla \cdot (\mathbf{v} \cdot \boldsymbol{\tau}) + \mathbf{v} \cdot \mathbf{S}_M + \mathbf{S}_H \tag{6}$$

In these equations, p, $\mathbf{v}$ and T stand for the mean pressure, velocity vector and temperature fields, respectively. Properties of air like dynamic viscosity (μ_{air}), density (ρ_{air}) and thermal conductivity (λ_{air}) also appear. Other terms seen in these equations are the source terms for momentum ($\mathbf{S}_M$) and enthalpy ($\mathbf{S}_H$), as well as the total enthalpy, $H_{tot} = H + \frac{1}{2}\mathbf{v}^2$. Note that, thanks to these equations, it is possible to resolve the flow fields (p, $\mathbf{v}$ and T) at every position and at any time once the equation of state for the fluid is known and the turbulence model is included.

With respect to turbulence modelling, in this work turbulence effects are introduced through the stress tensor:

$$\boldsymbol{\tau} = \mu_{air}\left(\nabla \mathbf{v} + (\nabla \mathbf{v})^T - \frac{2}{3}\,\delta\,\nabla \cdot \mathbf{v}\right) + \boldsymbol{\tau}_{\mathbf{R}} \tag{7}$$

where δ is the delta Kronecker function. In this work, the two-equation Shear Stress Transport (SST) model [58] will be used for an accurate description of the flow near the walls and in the bulk region. Accordingly, the Reynolds stress tensor, $\boldsymbol{\tau}_{\mathbf{R}}$, reads as:

$$\boldsymbol{\tau}_{\mathbf{R}} = \mu_T \left(\nabla \mathbf{v} + (\nabla \mathbf{v})^T\right) \tag{8}$$

where μ_T is the turbulent viscosity. These equations are solved numerically by using the Element-based Finite Volume Method [59] with a first-order algorithm for the discretization of turbulence equations and a high-resolution algorithm for the RANS discretization. More details on the implementation of the SST turbulence model and the numerical resolution of these equations can be found in the literature [60,61].

3.2. CFD simulation details

Fig. 1a shows the proposed domain geometry. The main gear (pinion, coloured in green) is placed centred in a cylindrical domain, with the secondary gear (wheel, coloured in red) centred at the corresponding location on the $z - axis$. To avoid undesirable effects of the boundary conditions on the CFD results near the region of interest, the axial extent of the domain is 15 times the pinion face width, and its diameter 10 times the pinion tip diameter. These limits clearly exceed the recommendations on domain limits (5 times the obstacle length if there is no wind across that direction) given by the COST guidelines for external flow simulations [55,62].

The domain is subdivided into small sub-volumes, with bigger elements on the borders of the domain and smaller ones near the main gear (see Fig. 1b). The distribution of the elements in the region between the gear teeth is structured for the pinion, with proper inflation layers near its walls to ensure that the normalized wall distance, y^+, remains below 1. After a grid convergence study [63,64], the resulting grid selected for the simulations is composed of 1,376,629 nodes.

With respect to the boundary conditions, the main gear surface is set as a non-slip wall at constant temperature. Boundary limits are set as openings so that air can freely enter or leave the domain.

The transient resolution involves the motion of the gears and their engagement. The main advantage of the proposed approach is that it does not need to update the sub-volumes after each iteration. First, the whole domain is defined as a non-inertial rotating domain. This implies the addition of source terms in the momentum equations, $\mathbf{S}_M$, to account for the Coriolis forces. Second, the secondary gear is included using the immersed boundary method (IBM [65]), i.e. introducing another set of source terms into the momentum equations to account for the effects of its motion. From the point of view of the non-inertial reference frame, this gear is orbiting the main gear while it rotates on its own axis. In this way, the gears engage properly and the air is expelled and suctioned before and after the engagement, respectively.

Note that this approach differs from those reviewed by Mastrone et al. [66], who compared several meshing approaches for the CFD simulation of gear transmissions. The overset, local and global remeshing approaches demand a huge computational cost in this case, especially in terms of time. The proposed global remeshing approach with mesh clustering could be of interest, as it is expected to reduce the computational time significantly. Unfortunately, it is not included in commercial packages or default OpenFOAM® distributions. The IBM by itself, as indicated by Burberi et al. [67], leads to inaccurate results due to the poor description of the mesh near the walls. Hence, this paper proposes a mixed approach that uses the IBM just for the wheel and a static mesh for the pinion thanks to the inclusion of the Coriolis terms. In this way, the near wall behaviour is modelled properly for the gear that is going to serve for the heat transfer coefficient calculations.

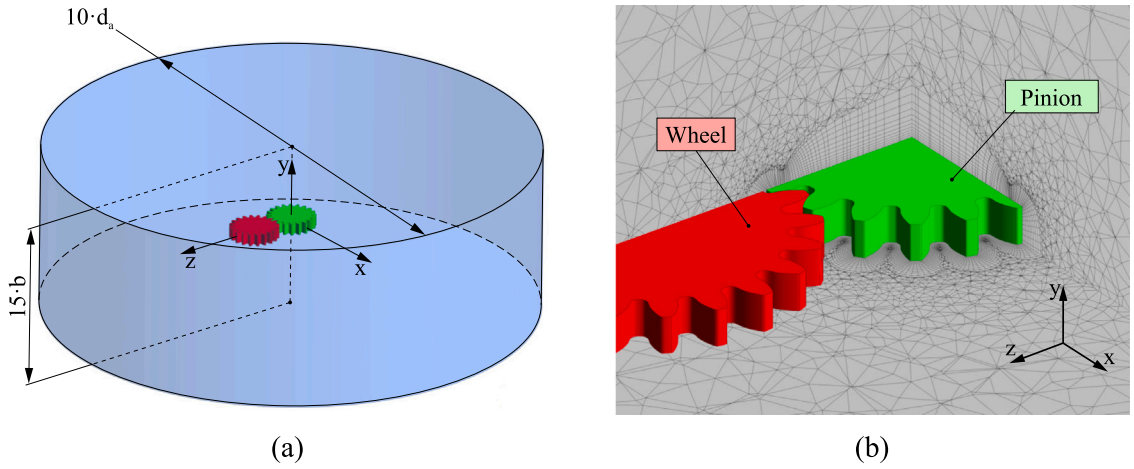

Fig. 1. Definition of the CFD model: (a) domain for the CFD analysis, and (b) a detail of the sub-volume discretization.

3.3. Calculation of the heat transfer coefficient from the CFD simulation results

The proposed numerical model provides the values for pressure, temperature and velocity vector for all the sub-volumes in the domain at any time step k. From these results, one can obtain three different definitions for the heat transfer coefficient over the main gear surfaces, and each of them will have a different meaning and purpose. The first one is an instantaneous local heat transfer coefficient (IL-HTC, $h_{i,k}$), which is calculated for each node i of the gear surfaces at a given time step k as follows:

$$h_{i,k} = \frac{q_{i,k}}{T_{i,k} - T_\infty} \tag{9}$$

where $q_{i,k}$ and $T_{i,k}$ are the heat flux and the temperature at node i and time step j, respectively.

The second definition corresponds to an instantaneous global heat transfer coefficient (IG-HTC, $\hat{h}_{j,k}$), which is calculated for a given gear surface j and time step k as follows:

$$\hat{h}_{j,k} = \frac{Q_{j,k}/A_j}{T_{j,k} - T_\infty} \tag{10}$$

where $Q_{j,k}$ is the thermal power released through surface j in time frame k, A_j is the area of surface j and $T_{j,k}$ is the average temperature of surface j in time frame k.

Finally, the third definition corresponds to a time-averaged global heat transfer coefficient (AG-HTC, $\hat{h}'_j$) that is calculated for each gear surface j as follows:

$$\hat{h}'_j = \frac{\omega}{2\cdot\pi} \cdot \sum_{k=2}^{n_{frame}} \frac{1}{2} \cdot (t_k - t_{k-1}) \cdot (\hat{h}_{j,k} + \hat{h}_{j,k-1}) \tag{11}$$

where ω is the angular speed of the gear, n_{frame} is the number of analysis frames during a revolution of the pinion and t_k is the time instant associated to analysis frame k. This AG-HTC is the one that should be considered to define the surface film conditions in the thermal finite element models of the gears.

4. Numerical examples and discussion of results

In this section the CFD model described in Section 3 is applied to derive a numerical heat convection model for a polymer spur gear transmission running in dry conditions, including the definition of the surface film conditions for the external boundary of the gear and the determination of the HTCs associated to each of them. This numerical heat convection model is used in Section 4.1 to investigate the influence of the face width and the input speed over the convective behaviour of the polymer gears. In Section 4.2, the results obtained from the numerical heat convection model are compared to those obtained from a classical heat convection model. Finally, in Section 4.3, an optimized heat convection model is proposed, which is aimed at improving the accuracy of the classical heat convection models but avoiding the elevated computational costs of the numerical heat convection model.

Table 1
Gear geometry and operating conditions for the nominal case study.

Parameter	Magnitude
Module, m	2 mm
Pressure angle, α	20°
Nominal face width, b	10 mm
Pinion teeth number, z_1	20
Wheel teeth number, z_2	20
Nominal input speed, ω_1	1000 rpm
Ambient temperature, T_∞	25 °C
Gear temperature, T	40 °C

Table 2
Thermal properties of the surrounding air at 25 °C.

Property	Magnitude
Thermal conductivity, λ_{air}	$2.61 \cdot 10^{-2}$ W/m/K
Kinematic viscosity, ν_{air}	$1.545 \cdot 10^{-5}$ m^2/s
Specific heat, cp_{air}	1004.4 J/kg/K
Density, ρ_{air}	1.185 kg/m^3
Thermal expansion, γ_{air}	$3.356 \cdot 10^{-3}$ 1/K

The study is conducted on a standard spur gear transmission whose macro geometry design parameters and nominal operating conditions are shown in Table 1. Both pinion and gear are considered to be made of polyoxymethylene (POM) and to be operating without lubricant. This gear transmission has been analysed with the CFD model described in Section 3 during twenty revolutions of the pinion, which is rotating at a nominal input speed ω_1 considering the thermal properties of the surrounding air given in Table 2. Note that the properties of the gear material are not of interest in this study, because the convective behaviour of the gears (and hence their HTCs) does not depend on them [68].

Fig. 2 shows a contour plot of the IL-HTC obtained over the pinion geometry, calculated using Eq. (9) for the last time frame of the CFD analysis. Here it is observed that the maximum values for the IL-HTC are produced at the tip and the sides of the leading surface, whereas the minimum values for the IL-HTC are obtained along the trailing surface. Fig. 2 also reveals that the gradients in the IL-HTC are relatively small within the great majority of the surfaces of the gear. The smallest gradients can be found at the side of the gear and the

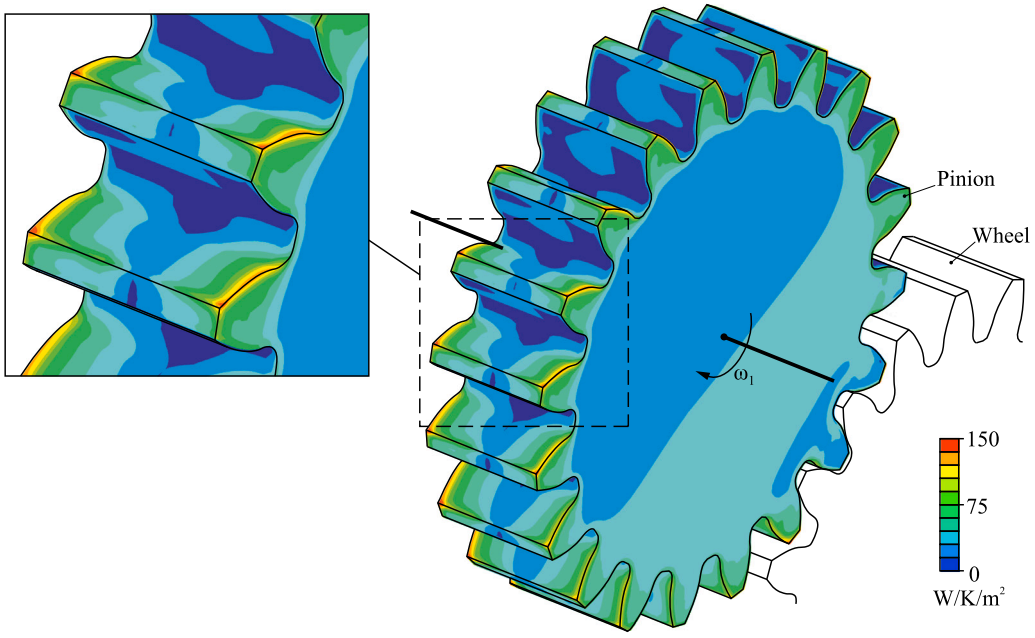

Fig. 2. Contour plot of the IL-HTC obtained from the CFD analysis for the nominal case study.

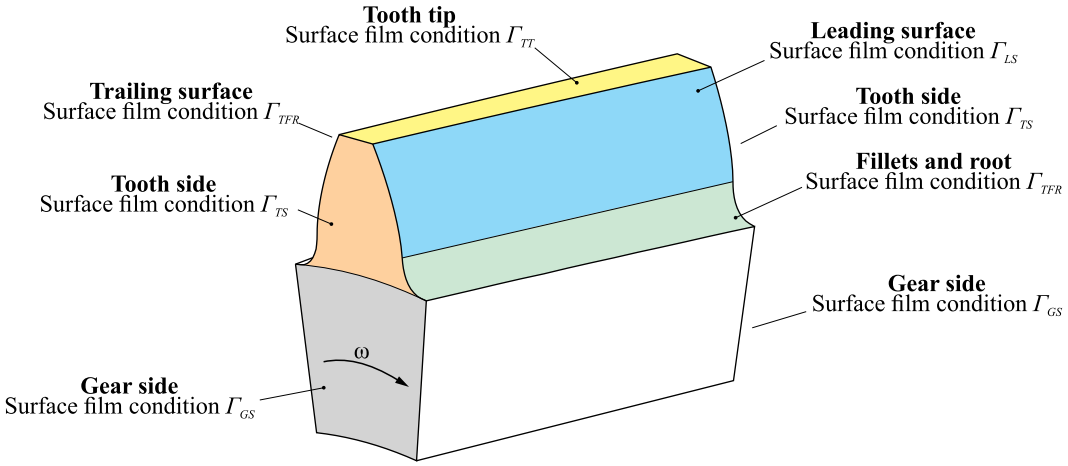

Fig. 3. Definition of the surface film conditions for the proposed convective heat transfer model.

largest gradients are observed in the leading surface and the tooth tip. The trailing surface, the fillets and the root have similar values for the IL-HTC, with small variations between them.

Observing the distribution of the IL-HTC over the pinion geometry, the decomposition into surface film conditions shown in Fig. 3 is proposed to study the convective phenomena in polymer spur gears. It consists of five surface film conditions: surface film condition Γ_{GS} is specified for the gear sides, surface film condition Γ_{TS} is specified for the tooth sides, surface film condition Γ_{TT} is specified for the tooth tip, surface film condition Γ_{LS} is considered for the leading surface and surface film condition Γ_{TFR} is considered for the rest of the surfaces (trailing surface, fillets and root).

The convective behaviour observed in Fig. 2 can be better understood by analysing the air flow streams that are produced in the vicinity of the pinion geometry, which are shown in Fig. 4. Note that these streams correspond to streamlines computed from the non-inertial velocity fields. Accordingly, despite the clockwise motion of the gear, these streams are seen as anticlockwise from the rotating system of reference. Also note that, for the sake of clarity, only the streams corresponding to one of the sides of the gear are drawn. A similar behaviour can be found on the opposite side of the gear. From this figure, the formation of four different air streams is apparent, which are denoted as Ω_{GS}, Ω_{TT}, Ω_{LS} and Ω_{TFR}. These streams are driven by three phenomena:

1. When the pinion teeth engage the gear teeth, the air inside the gear pockets is expelled. After engagement, the separation of the teeth induces a vacuum inside the gear pockets that produces a quick suction of the surrounding air.
2. This suction is sustained after the engagement thanks to the gear rotation. As in Shockwave Power Reactors [69], the rotation at high angular frequencies induces a centrifugal hydrostatic pressure field inside the pockets. In this case, the pressure drop inside the pocket gears can be estimated as:

$$\Delta p = -\rho_{air} \cdot \omega^2 \cdot ln\left(\frac{d_a}{d_f}\right) \tag{12}$$

   where d_a is the tip diameter and d_f the root diameter.
3. Finally, the friction of the air with the sides of the rotating gear induces a swirl of the surrounding air.

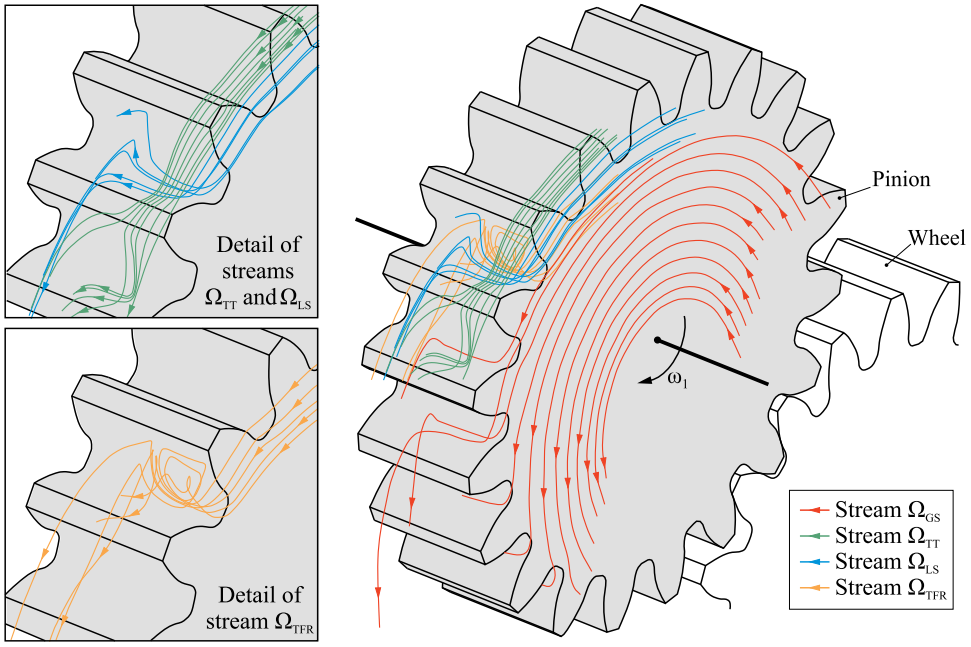

Fig. 4. Air flow streams obtained from the CFD analysis for the nominal case study.

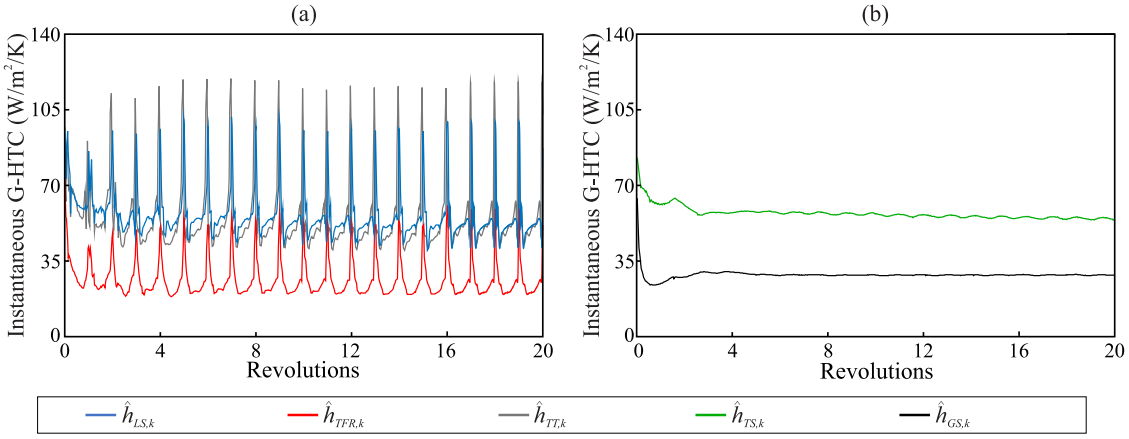

Fig. 5. Evolution of the IG-HTC during the CFD analysis: (a) surface film conditions Γ_{LS}, Γ_{TFR} and Γ_{TT}, and (b) surface film conditions Γ_{TS} and Γ_{GS}.

These three phenomena explain the overall flow behaviour surrounding the gears. To sum up, fresh air approaches the gear following the stream Ω_{GS}. This stream comes parallel to the rotation axis and starts to swirl as it approaches both sides of the gear. As this stream advances, it starts to approach the gear pockets. Once this stream reaches the pockets, it separates into two streams: Ω_{LS} and Ω_{TFR}. The Ω_{LS} stream impacts onto the leading surface and causes it to cool. The Ω_{TFR} stream has a huge swirling component so it does not reach the leading surface. Instead, it attaches to the trailing surface, being responsible for its cooling. These two streams collide with similar streams coming from the other side of the gear so they are all expelled from the pockets over the tooth tips. These streams remain close to the gear teeth forming the Ω_{TT} stream, which comes from the air expelled from the gear pockets.

A more convenient way to examine the convective cooling in these surfaces is through global heat transfer coefficients. Fig. 5 shows the evolution of the IG-HTC (as given by Eq. (10)) for these surfaces, where it can be observed that in all cases the IG-HTC suffers a transient period when the analysis is started. After a few revolutions of the pinion, this transient period ends and the IG-HTC tends to stabilize, reaching a steady state that is repeated approximately for each revolution of the pinion.

Fig. 6 shows in greater detail the evolution of the IG-HTC during the last revolution of the analysis, for each of the surface film conditions considered. The areas shaded in grey represent the parts of the gear cycle where the pinion tooth is engaged with the corresponding gear tooth. This figure also shows the AG-HTC calculated using Eq. (11). It can be observed that both the IG-HTC and the AG-HTC are larger for surface film condition Γ_{LS} (Fig. 6a) than for surface film condition Γ_{TFR} (Fig. 6b) during the entire rotation of the pinion. As explained before, since the cool air impacts mostly on the leading surface (see Fig. 4), it produces a greater convective cooling than for the trailing surface. This fact contradicts the assumption made in Černe's convective model [39], where the same heat transfer coefficient is assumed for both surfaces.

Moreover, it can be observed that, for the great majority of the gear cycle, the IG-HTC and the AG-HTC at the tooth tip (Fig. 6c) are closer to those of the leading surface (Fig. 6a) than to that of the trailing surface (Fig. 6b). For these three surfaces, the IG-HTC and the AG-HTC are quite similar during the entire gear cycle, except for that part of the gear cycle in which the observed pinion tooth engages with the corresponding wheel tooth, where an increase in the IG-HTC is observed. Fernandes [36] contemplated this effect in his work by

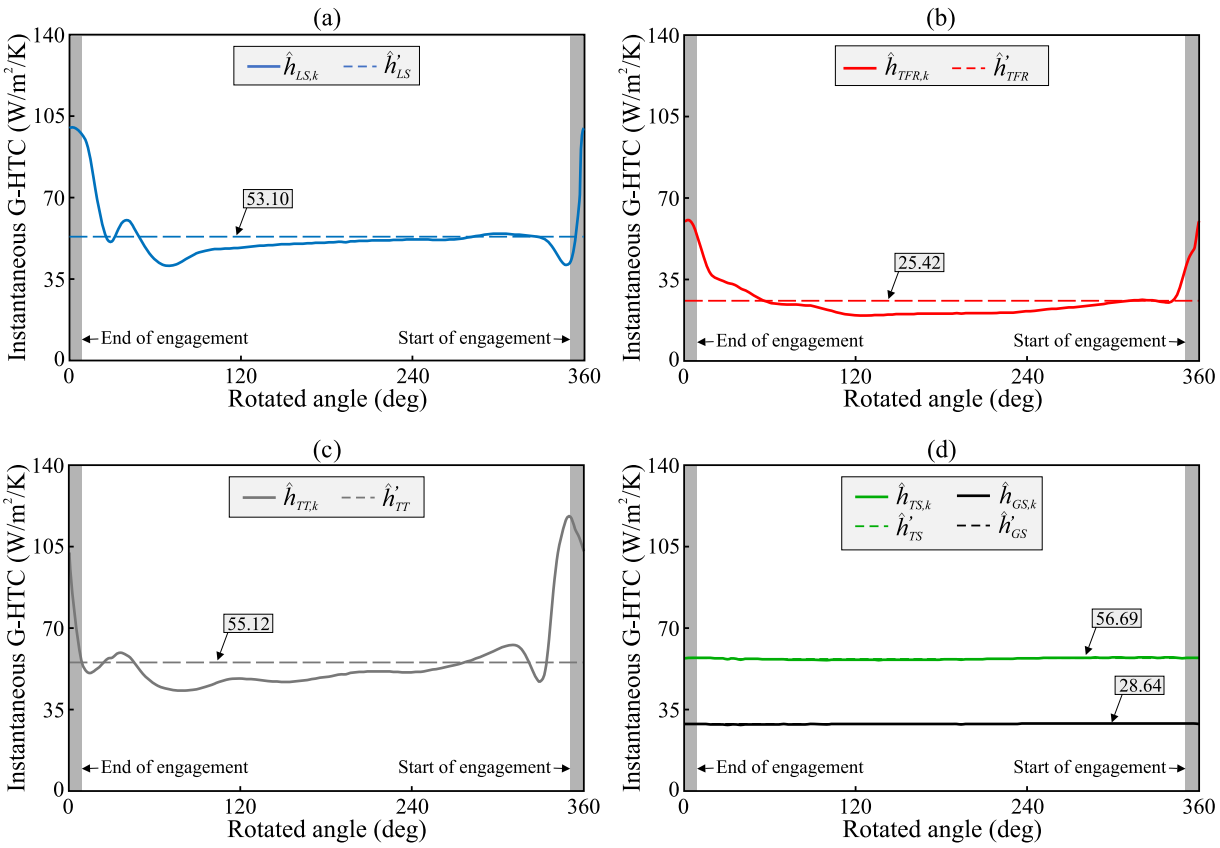

Fig. 6. Evolution of the IG-HTC during the last revolution of the CFD analysis: (a) surface film condition Γ_{LS}, (b) surface film condition Γ_{TFR}, (c) surface film condition Γ_{TT}, and (d) surface film conditions Γ_{TS} and Γ_{GS}. A dashed line indicates the AG-HTC for each surface film condition considered.

determining the heat transfer coefficient for the leading surface as the time-averaged heat transfer coefficient of this surface during and out of the meshing. However, he understood that the convection conditions of the leading surface were similar to those of the trailing surface when the tooth is out of the meshing, but these results reveal that this assumption may not be totally accurate.

Finally, Fig. 6d shows the IG-HTC and the AG-HTC for the surface film conditions Γ_{TS} and Γ_{GS}. Here it is observed that, during the entire rotation of the pinion, both IG-HTC and AG-HTC of the tooth side are larger than those of the gear side. This fact reasserts the consideration made by Černe [39] of splitting the side of the gear into two different surface film conditions. For both surface film conditions, the IG-HTC and the AG-HTC are almost coincident, demonstrating that only small fluctuations are produced in these heat transfer coefficients during the gear cycle.

4.1. Evolution of the heat transfer coefficient with the input speed and the face width

The heat transfer coefficient of the external surfaces of a polymer spur gear depends on their geometry, the relative motion between these surfaces and the surrounding air, and the thermal properties of this air [50]. On the one hand, the geometry of the surfaces of a standard spur gear is defined by the parameters of the basic rack (modulus, pressure angle, addendum and dedendum coefficients, and fillet radius), the number of teeth and the face width of the gear. On the other hand, the relative motion between the air and the surfaces of the gear depends mostly on its angular speed and the type of flow. This means that there are a great number of variables that may have some effect on the heat transfer coefficient of the gear surfaces, and it would be interesting to understand the relation between these variables and the heat transfer coefficients that regulate the convective behaviour of the gear.

For the sake of brevity, in this section only the influence of the face width and the input angular speed on the AG-HTC is studied. The angular speed of the gears affects the Reynolds number that drives the convective behaviour of the gear surfaces, as indicated by Eqs. (2) and (3). The face width of the gears affects the convective heat dissipation [5,70] because it changes the geometry of the gear surfaces in a significant way. However, the face width of the gears is seldom considered in the convective heat dissipation models found in the literature [15,36].

Thus, to conduct this study, different variations of the case study described in Table 1 have been investigated, in which various combinations of the face width and the nominal input speed are performed. To obtain such variations, four different values of the face width $b = [5, 10, 15, 20]$ mm and four different input angular speeds $\omega_1 = [500, 1000, 1500, 2000]$ rpm are considered. For each of these variations, the AG-HTC is calculated for each of the surface film conditions described in Fig. 3.

Fig. 7 shows the AG-HTC as a function of the input speed and the face width, for each of the surface film conditions considered. The black dots indicate those combinations that have been studied, and the isolines are interpolated from the results of the cases studied. In all the surface film conditions it is observed that the heat transfer coefficient tends to increase with the angular speed of the gears. This is somewhat expected, as the faster the gear rotates, the greater the relative velocity between the gear and the surrounding fluid is, thereby increasing its capacity to cool down the gear.

The results also show a certain dependency of the heat transfer coefficient on the face width of the gears, with different degrees of influence depending on which surface is considered. For surface film conditions Γ_{TT} and Γ_{TS} (Fig. 7a and d), the dependency of the heat transfer coefficient with respect to the face width of the gear is relatively small. The rest of the surfaces exhibit a larger dependency on

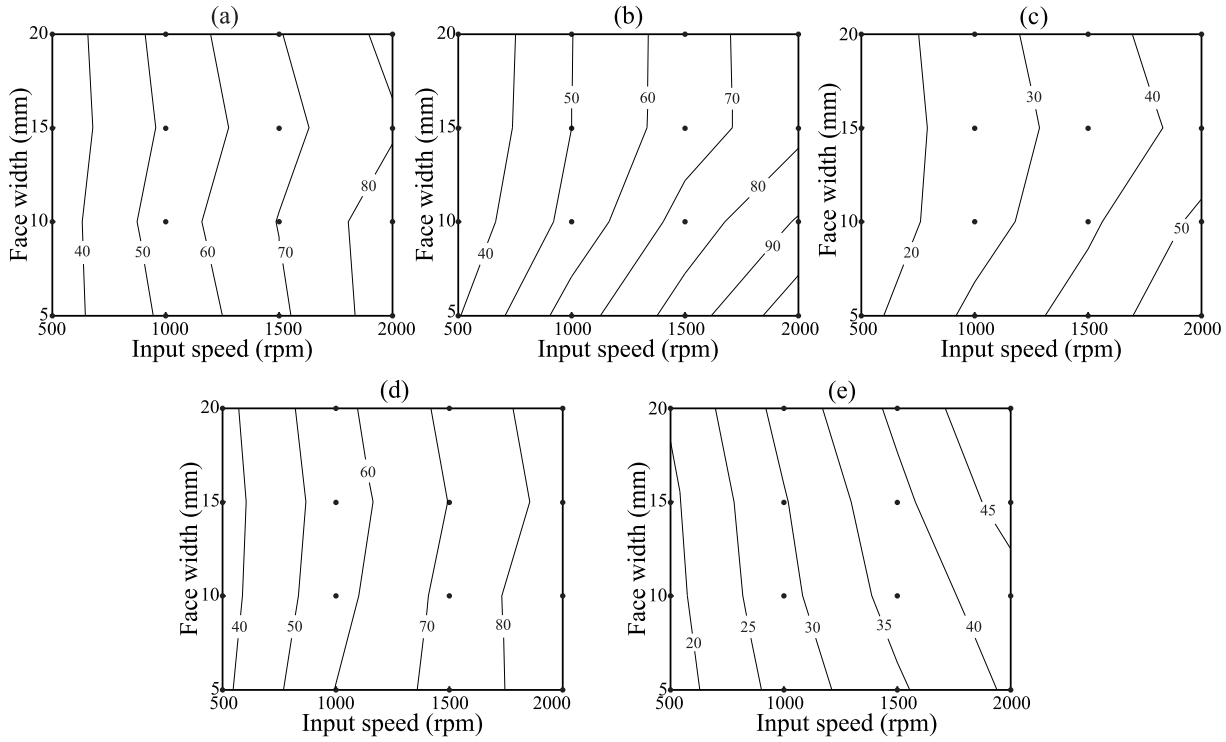

Fig. 7. Evolution of the AG-HTC as a function of the input speed and the face width, calculated using the numerical heat convection model for surface film conditions (a) Γ_{TT}, (b) Γ_{LS}, (c) Γ_{TFR}, (d) Γ_{TS} and (e) Γ_{GS}. The AG-HTC values are given in W/m^2/K. The black dots indicate those combinations of input speed and the face width that have been studied.

the heat transfer coefficient with respect to the face width of the gears, especially for larger rotational speeds. This is because the cold air that enters the gear pockets travels along the face width of the gears so that the larger the face width is, the higher the convection cooling through these surfaces will be.

The observations made in the previous section hold in all these cases. For all of them, the largest heat transfer coefficient is obtained at the leading surface and the lowest heat transfer coefficient is produced at the gear side and the trailing surface. In all cases, the heat transfer coefficient of the tooth tip is similar to that of the leading surface.

4.2. Comparison of the classical heat convection models to the numerical heat convection model

Classical heat convection models have the advantage of being simpler and more computationally efficient than the numerical heat convection models, but it is not clear whether they are able to reproduce the actual convective phenomena that occur in polymer spur gear transmissions running in dry conditions. In order to gain some insight into this question, in this subsection the HTCs calculated from a classical heat convection model are compared to those calculated using the numerical heat convection model described in Section 3.

Among the classical heat convection models available in the literature, the one proposed by Černe [39] (described in detail in Appendix) was selected to perform this comparison, because it is one of the most advanced heat convection models found in the literature. The black isolines in Fig. 8 show the HTCs calculated using Černe's model as a function of the angular speed and the face width of the gears, for each of the surface film conditions considered. Here it is observed that all HTCs increase with the input speed of the transmission, since Eq. (3) depends on the Reynolds number that is a function of the input speed. In contrast, Černe's HTCs are independent of the face width, since this magnitude is not involved in the calculations. It is important to mention that in this figure the HTCs for surface film conditions Γ_{TT}, Γ_{LS} and Γ_{TFR} are identical, as this set of surfaces constitutes a single surface film condition in Černe's model (Γ_f in Fig. A.10).

To quantify the degree of similarity between the HTCs calculated using Černe's convective model and using the numerical model, two different deviation magnitudes are defined:

- The deviation δ_j is defined as the difference between a given value of heat transfer coefficient h_j (for surface j, face width b and input velocity ω_1) and the time-averaged global heat transfer coefficient $\hat{h}'_j$, which is used as a reference value and is calculated from the numerical model using Eq. (11):

$$\delta_j\left(b,\omega_1\right) = h_j\left(b,\omega_1\right) - \hat{h}'_j\left(b,\omega_1\right) \tag{13}$$

- The relative deviation ε_j is defined as the ratio between the deviation δ_j and the time-averaged global heat transfer coefficient $\hat{h}'_j$ calculated from the numerical model using Eq. (11):

$$\varepsilon_j\left(b,\omega_1\right) = \frac{\delta_j\left(b,\omega_1\right)}{\hat{h}'_j\left(b,\omega_1\right)} \tag{14}$$

The coloured regions in Fig. 8 show the relative deviation of Černe's heat transfer coefficients compared to those calculated from the numerical model. Let us recall that a positive relative deviation implies that Černe's model overestimates the amount of heat dissipated by convection, whereas a negative relative deviation implies that Černe's model underestimates it.

The results obtained for surface film conditions Γ_{TT} (Fig. 8a) and Γ_{LS} (Fig. 8b) indicate that, for the great majority of the design space considered, Černe's model tends to underestimate the amount of heat dissipated by convection through these surfaces, especially at high input speeds. Conversely, the results obtained for surface film condition Γ_{TFR} (Fig. 8c) indicate that Černe's model tends to overestimate the amount of heat dissipated by convection through this surface, especially at low input speeds. Surface film condition Γ_{TFR} is where the

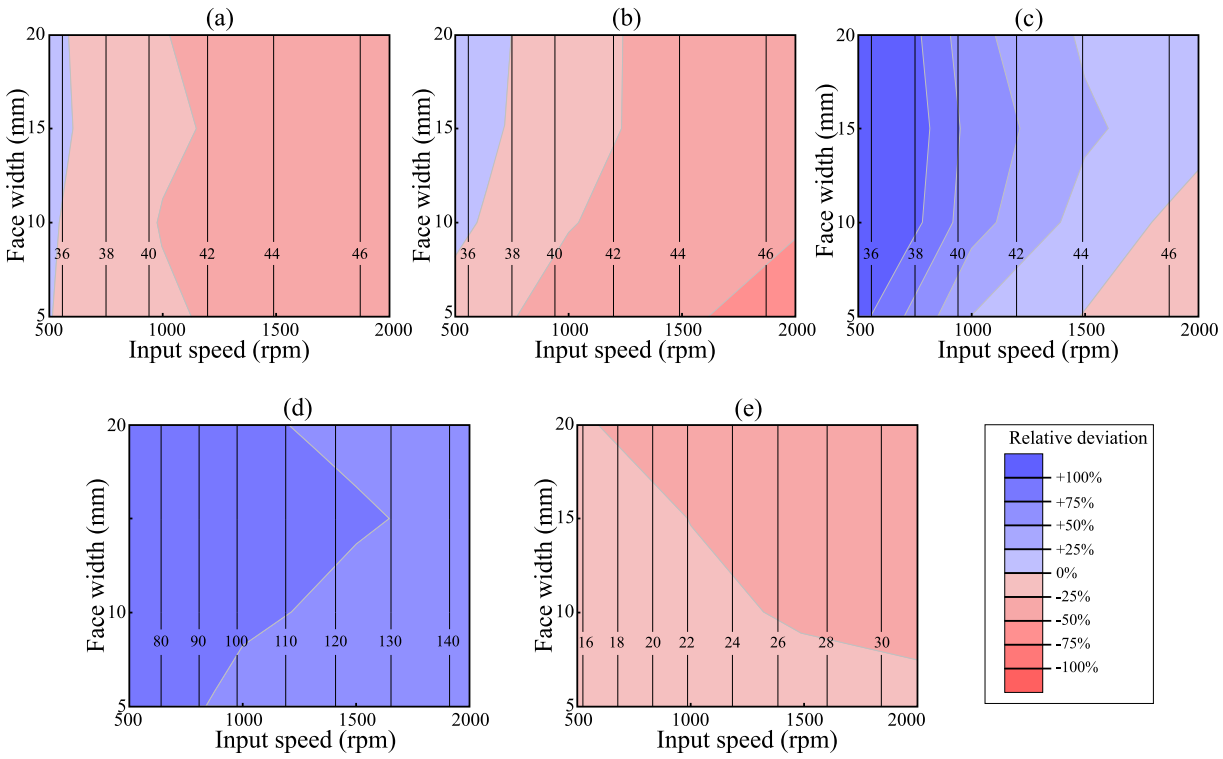

Fig. 8. Evolution of the HTC as a function of the input speed and the face width, calculated using Černe's heat convection model for surface film conditions (a) Γ_{TT}, (b) Γ_{LS}, (c) Γ_{TFR}, (d) Γ_{TS} and (e) Γ_{GS}. The HTC values are given in W/m^2/K. The colour scale indicates the relative deviation of these results with respect to the results of the numerical heat convection model.

largest relative errors (understood as the absolute value of the relative difference between the two models) are produced.

In these surface film conditions (Γ_{TT}, Γ_{LS} and Γ_{TFR}) the differences in the heat transfer coefficients calculated using both models arise because the type of air flow considered in the derivation of the coefficients given in Table A.5 does not represent the actual flow observed in the numerical results (Fig. 4). In Černe's model, these surfaces were viewed as semi-cylindroids positioned inside an air crossflow, which does not coincide with the type of relative motion between the air and these surfaces in Fig. 4.

Regarding surface film condition Γ_{TS} (Fig. 8d), the results obtained indicate that Černe's model tends to overestimate the amount of heat dissipated by convection through these surfaces, especially at low speeds and large face widths. In this case, the type of flow considered in the calculation of the coefficients given in Table A.5 (plates with the airflow parallel to them) is similar to the type of flow observed in the numerical results (Fig. 4). In spite of this similarity, notable deviations exist between the heat transfer coefficients calculated using both models, which could be attributed to the fact that the gear pockets reduce the amount of cool air that effectively comes into contact with the tooth sides, thus reducing their convective cooling capacity.

Finally, the results obtained for the surface film condition Γ_{GS} (Fig. 8e) indicate that Černe's model tends to underestimate the amount of heat dissipated by convection in these regions of the gear, especially at high speeds and large face widths. This is the surface film condition in which the relative errors are smaller, and they could be attributed to the fact that the coefficients given in Table A.5 for these surfaces were derived for a $Pr = 0.74$ [71], whereas the Prandtl number in this work is $Pr = 0.70$.

4.3. Optimized heat convection model for polymer spur gears

As has been observed in the previous subsection, and due to the simplicity of its calculation hypotheses, Černe's heat convection model has limited capabilities to provide accurate HTCs for some of the surface film conditions in which the gear is decomposed (see Fig. 3). Inaccuracies in the calculation of the convective behaviour of the gears lead to errors in the prediction of their operating temperature, which ultimately affect the estimated life of the polymer gear transmission. For this reason, it is interesting to obtain an optimized convective model capable of providing a better approximation to the actual convective behaviour of the polymer gears.

In this subsection a new optimized heat convection model for polymer spur gear transmissions is proposed, in which Eqs. (2) and (3) are applied to calculate the heat transfer coefficient for each of the surface film conditions shown in Fig. 3:

- The characteristic length for each surface film condition is selected according to the direction of the air flow observed in Fig. 4. In this way:
  - The characteristic length for surface film condition Γ_{TT} has been selected as the transverse tooth thickness at the tip circle (s_a).
  - The characteristic length for surface film conditions Γ_{LS} and Γ_{TFR} has been selected as half the face width of the gear ($b/2$).
  - The characteristic length for surface film condition Γ_{TS} has been selected as the tooth width at the reference circle (s_k).
  - The characteristic length for surface film condition Γ_{GS} has been selected as the reference radius of the gear ($d/2$).
- The Reynolds number for each surface film condition has been calculated by approximating the relative velocity of the air (v_{air}) to the velocity that the air would have in the middle of such a surface.
- A constant coefficient $C_3 = 0.333$ has been selected for all surface film conditions.

Table 3
Summary of the optimized convective heat transfer model and the values for the coefficients C_1 and C_2 obtained from the optimization process for each surface film condition.

Film cond.	L_c	v_{air}	Re	C_3	C_1	C_2
Γ_{TT}	s_a	$\frac{\omega \cdot d_a}{2}$	$\frac{L_c \cdot v_{air}}{\nu_{air}}$	0.333	0.108	0.645
Γ_{LS}	$\frac{b}{2}$	$\frac{\omega \cdot d}{2}$	$\frac{L_c \cdot v_{air}}{\nu_{air}}$	0.333	0.089	0.748
Γ_{TFR}	$\frac{b}{2}$	$\frac{\omega \cdot d}{2}$	$\frac{L_c \cdot v_{air}}{\nu_{air}}$	0.333	0.027	0.829
Γ_{TS}	s_k	$\frac{\omega \cdot d}{2}$	$\frac{L_c \cdot v_{air}}{\nu_{air}}$	0.333	0.196	0.605
Γ_{GS}	$\frac{d}{2}$	$\frac{\omega \cdot d}{2}$	$\frac{L_c \cdot v_{air}}{\nu_{air}}$	0.333	0.174	0.630

Table 4
Summary of minimum relative deviations, maximum relative deviations and the RMS of the deviation for Černe's and optimized heat convection models, with respect to the results of the numerical model.

Film cond.	Černe convective model			Optimized convective model		
	$\min(\delta_j)$	$\max(\delta_j)$	RMS_j	$\min(\delta_j)$	$\max(\delta_j)$	RMS_j
Γ_{TT}	−45.8%	5.7%	10.3	−3.6%	5.5%	0.8
Γ_{LS}	−56.3%	18.2%	12.2	−9.7%	6.5%	1.0
Γ_{TFR}	−20.0%	159.6%	6.0	−4.8%	12.6%	0.8
Γ_{TS}	62.7%	99.2%	21.3	−5.9%	3.6%	0.6
Γ_{GS}	−37.5%	−11.0%	4.4	−9.8%	10.9%	1.1

In addition to these magnitudes, the application of Eqs. (2) and (3) requires the specification of coefficients C_1 and C_2, which need to be adjusted for each surface film condition defined on the gear. In order to do so, in this work an optimization process has been followed in which C_1 and C_2 are selected in such a way that they minimize the root mean square value of the deviation of the calculated heat transfer coefficients and the AG-HTC obtained from the numerical model. For this purpose, the root mean square of the deviation is defined as:

$$RMS_j = \sqrt{\frac{1}{n}\sum_{i=1}^{n}\left[\delta_j\left(b_i, \omega_{1i}\right)\right]^2} \tag{15}$$

where δ_j is the deviation as defined by Eq. (13), n is the total number of case studies, and b_i and ω_{1i} are the face width and the input speed for each case study, respectively. The optimization process is conducted using a conventional Newton–Raphson scheme. The resulting values for the coefficients C_1 and C_2, with the rest of the parameters for the application of Eqs. (2) and (3), are shown in Table 3.

Considering the optimized values for C_1 and C_2, the heat transfer coefficients for the surface film conditions of Fig. 3 have been recalculated, and the results are shown by the isolines in Fig. 9. The coloured regions in Fig. 9 show the relative deviation ε_j of the optimized heat transfer coefficients compared to those calculated from the numerical model. Note that the colour scale used in this figure is different to the one used in Fig. 9 to indicate the different amplitude in the deviations. Here it is observed that by considering the face width as the characteristic length for surface film conditions Γ_{LS} and Γ_{TFR}, the HTCs of these surfaces has become dependent on the face width, imitating the convective behaviour observed in Fig. 7.

Table 4 summarizes the minimum and maximum relative deviations of the optimized heat convection model with respect to the results of the numerical model. The table also shows the minimum and maximum relative deviations of Černe's model with respect to the results of the numerical model. Considering all the surface film conditions, the maximum relative error of the optimized model is 10.9% (surface film condition Γ_{GS}), whereas the maximum relative error of Černe's model is 159.6% (surface film condition Γ_{TFR}). The table also shows the RMS of the deviation of both models with respect to the numerical model. Here it is observed that, compared to Černe's model, the optimized model reduces the RMS by one order of magnitude.

To sum up, the CFD simulations presented in this work provide a good insight into the air flow organization around the gears. The analysis of the flows near each surface made it possible to provide a suitable correlation for the corresponding HTC. The correlations provided should be enhanced in future work with experimental data to validate the proposed CFD model. This validation could be addressed by using two different experimental approaches: thermal analysis with infrared cameras, and flow analysis with particle image velocimetry.

Infrared cameras have been used in the past by Černe [39,72] and Letzelter [73] to assess the running temperature of polymer gears. Although this is an interesting method to validate the temperature results obtained from computer simulations, its utility for the validation of the results obtained in this work is not clear, because the heat convection effect cannot be studied independently from other effects (frictional heat generation, hysteretic heat generation, radiation, etc.) that have an important impact on the temperature of the gears. To provide an example, a mismatch in the temperature prediction could be produced either by a higher value for the coefficient of friction (which increases the heat generation) or by a lower value for the HTCs (which reduces the heat dissipation).

Particle Image Velocimetry has been previously used to measure the flow around gear boxes [43] and gear pumps [74]. However, as explained by Mastrone [43], this validation is more qualitative than quantitative. Moreover, this technique is able to assess the air flow around the gears, but it is unable to measure the heat dissipated from them by convection. In short, it can be said that the experimental validation of these results is not straightforward, and a combination of techniques may be required for such a purpose. For this reason, this task is left for future work.

As a final remark, these results should not be extrapolated to any other case studies. Further research should be conducted in order to confirm the validity of these results for spur gear geometries obtained from different basic racks and numbers of teeth.

5. Conclusions

This work is devoted to study the convective heat transfer phenomenon in polymer spur gears running in dry conditions. For such a purpose, a numerical heat convection model based on a CFD analysis of the transmission has been developed, in which a detailed simulation of the polymer gears in operating conditions is conducted. The results obtained from this numerical model have allowed us to study the formation of the air flow around the gears, and to determine three different versions of the heat transfer coefficients for the external surfaces of the gears that are denoted as IL-HTC, IG-HTC and AG-HTC.

The performance of this numerical model has been demonstrated with a set of case studies, where different variations of a polymer spur gear transmission have been considered, in which the input angular speed and the face width of the gears have been varied.

The results achieved from the proposed numerical model have been compared to those obtained following the classical heat convection model proposed by Černe, revealing that the relative deviation of Černe's model with respect to the numerical model can be as high as 125% for the leading and trailing surfaces, but it is below 50% for the rest of the gear surfaces. These differences could be attributed to the divergences between the type of flow assumed in the derivation of Černe's model and the actual air flow.

In order to reduce these differences, an optimized heat convection model has been derived, in which empirical equations based on the Newton's law of cooling are used to determine the heat transfer coefficient for the external surfaces of a polymer gear. With these new equations, the relative differences with respect to the results obtained from the numerical method are smaller than 10%, thus enhancing the accuracy of the classical heat convection model.

Further work on this topic could be directed towards studying the variation of the heat transfer coefficient with the design parameters of the basic rack or the number of teeth of the gears. Moreover, by extending these methodologies to other types of gears (helical gears, bevel gears, etc.), more accurate predictions of the heat transfer coefficients could be obtained, which would reduce the temperature errors committed in the temperature calculations.

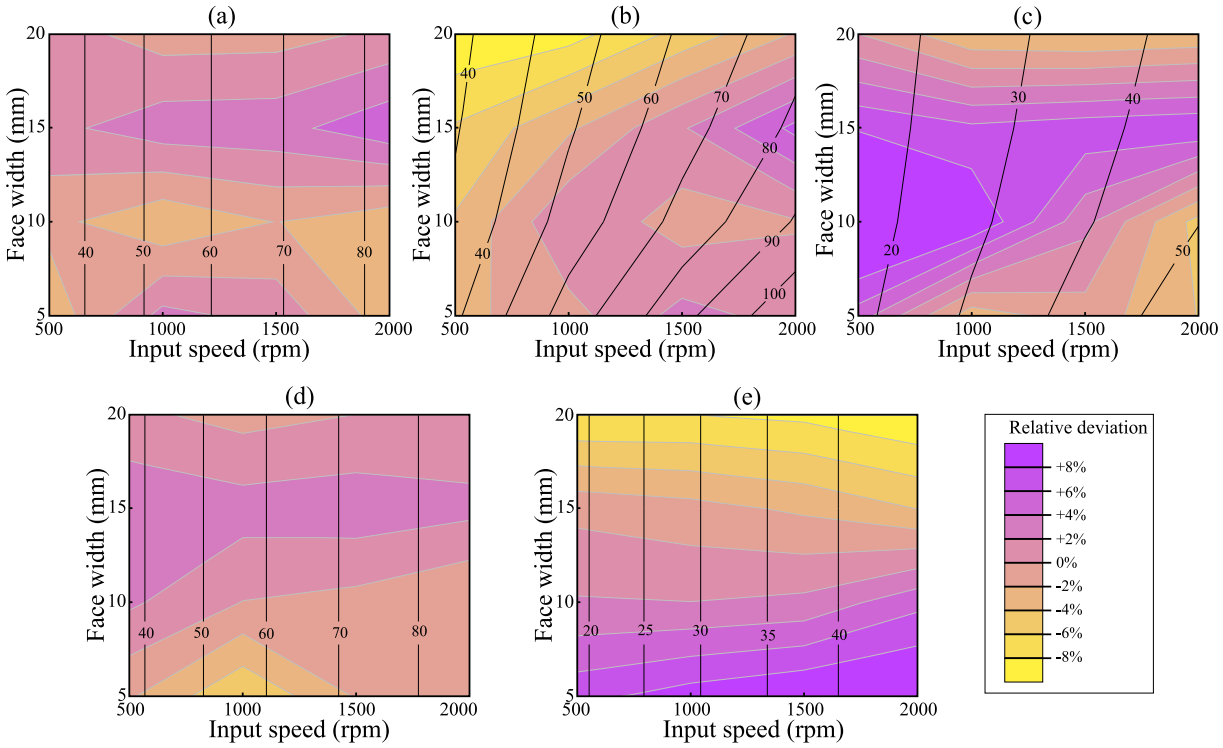

Fig. 9. Evolution of the HTC as a function of the input speed and the face width, calculated using the optimized heat convection model for surface film conditions (a) Γ_{TT}, (b) Γ_{LS}, (c) Γ_{TFR}, (d) Γ_{TS} and (e) Γ_{GS}. The HTC values are given in W/m^2/K. The colour scale indicates the relative deviation of these results with respect to the results of the numerical heat convection model.

CRediT authorship contribution statement

Victor Roda-Casanova: Conceptualization, Formal analysis, Investigation, Writing – original draft. **Francisco Sanchez-Marin:** Resources, Writing – review & editing. **Raul Martinez-Cuenca:** Methodology, Software, Validation, Investigation, Writing – review & editing.

Declaration of competing interest

The authors declare that they have no known competing financial interests or personal relationships that could have appeared to influence the work reported in this paper.

Data availability

No data was used for the research described in the article.

Funding

This research did not receive any specific grant from funding agencies in the public, commercial or not-for-profit sectors.

Appendix. Černe's convective heat transfer model

In this section a classical heat convection model for spur polymer gears (proposed by Černe [39]) is analysed in depth, in order to provide the reader with further understanding of the calculation of the heat transfer coefficients for polymer spur gears based on approximating the external surfaces of the gear to simple geometrical objects. This convective heat transfer model is summarized in Fig. A.10, where three different surface film conditions are considered for the external surfaces of the gears: Γ_f, Γ_G and Γ_i. The heat transfer coefficients for these surface film conditions are calculated using Eqs. (2) and (3) combined with the parameters given in Table A.5.

Table A.5
Heat transfer coefficients for the surface film conditions of Černe's convective model [39].

Film cond.	C_1	C_2	C_3	L_c	v_{air}	Re	Ref. object
Γ_f	3.800	0.200	0.333	$d_a - d_f$	$\frac{\omega \cdot d}{2}$	$\frac{L_c \cdot v_{air}}{\nu_{air}}$	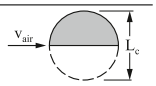
Γ_G	0.664	0.500	0.333	s_t	$\frac{\omega \cdot d}{2}$	$\frac{L_c \cdot v_{air}}{\nu_{air}}$	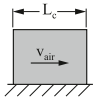
Γ_i	0.326	0.500	0.000	$\frac{d}{2}$	$\frac{\omega \cdot d}{2}$	$\frac{L_c \cdot v_{air}}{\nu_{air}}$	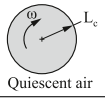 Quiescent air

Surface film condition Γ_f is characterized by the convective heat transfer coefficient h_f and applied to the set of surfaces consisting of the leading surface, the trailing surface, the tooth tip, the fillets and the root. For the calculation of this heat transfer coefficient, this set of surfaces was viewed as a semi-cylindroid (with a radius equal to the tooth depth) positioned inside an air crossflow. Under this assumption, h_f was calculated as proposed by Knudsen [75] using the coefficients given in Table A.5.

Surface film condition Γ_G is applied at the tooth sides and characterized by the convective heat transfer coefficient h_G. For the calculation of this heat transfer coefficient these surfaces were viewed as plates (with a characteristic length equal to the transverse tooth thickness at the reference circle) with the airflow parallel to them. Under this assumption, h_G was calculated as given by Holman [21] using the coefficients shown in Table A.5. These coefficients are valid for Reynolds numbers under $5 \cdot 10^5$.

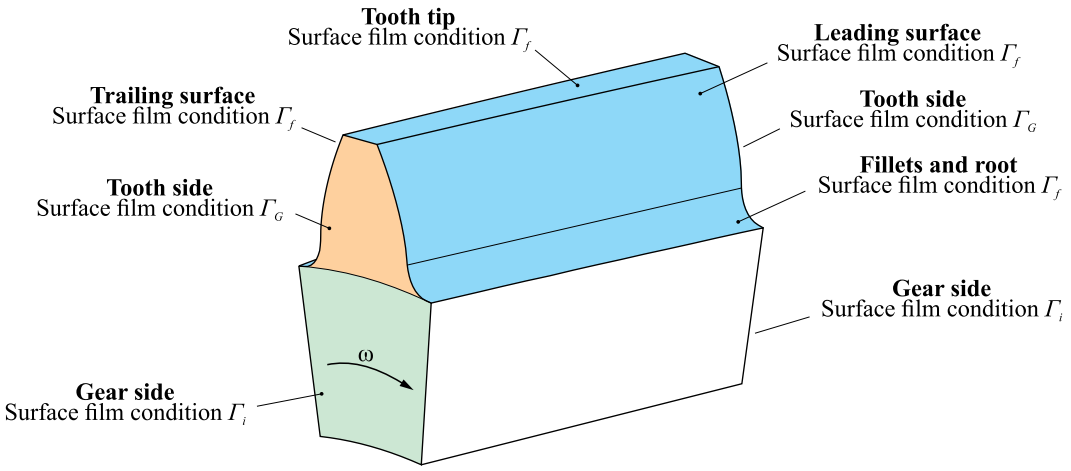

Fig. A.10. Definition of surface film conditions for the convective heat transfer model proposed by Černe [39].

Finally, **surface film condition** Γ_i is applied to the sides of the gear and characterized by the convective heat transfer coefficient h_i. For the calculation of this heat transfer coefficient, these surfaces were viewed as the sides of a disc rotating in quiescent air. Under this assumption, h_G was calculated as proposed by Millsaps and Pohlhausen [71,76] using the coefficients given in Table A.5, which are valid for Reynolds numbers in the interval $Re \in \left[2,\ 2 \cdot 10^6\right]$ and a $Pr = 0.74$. The results given by Millsaps and Pohlhausen show that the heat transfer coefficient at the gear sides is independent of the position in which it is calculated.

References

[1] Kalin M, Kupec A. The dominant effect of temperature on the fatigue behaviour of polymer gears. Wear 2017;376–377:1339–46. http://dx.doi.org/10.1016/j.wear.2017.02.003.

[2] Koffi D, Gauvin R, Yelle H. Heat generation in thermoplastic spur gears. Trans ASME, J Mech Des 1985;107(1):31–6. http://dx.doi.org/10.1115/1.3258688.

[3] Hachmann H, Strickle E. Polyamide als zahnradwerkstoffe. Konstruktion 1966;18(3):81–94.

[4] VDI-2736 blatt 2: thermoplastic gear wheels - cylindrical gears - calculation of the load-carrying capacity. Standard, Dusseldorf, DE: Verein Deutscher Ingenieure; 2013.

[5] Takanashi S, Shoji A. Uber den temperaturanstieg von zahnen von kunststoffzahnradern (2. bericht): Uber die gleichgewichtstemperatur von zahnen von kunststoffzahnrader. Sci Rep Res Inst Tokohu Univ 1979;28:103–15.

[6] Mao K. The performance of dry running non-metallic gears (Ph.D. thesis), School of Manufacturing and Mechanical Engineering, The University of Birmingham; 1993.

[7] Blok H. The flash temperature concept. Wear 1963;6:483–94.

[8] Roda-Casanova V, Fernandes C. A comparison of analytical methods to predict the bulk temperature in polymer spur gears. Mech Mach Theory 2022;173:104849. http://dx.doi.org/10.1016/j.mechmachtheory.2022.104849.

[9] Yusuf T, Mabood F. Slip effects and entropy generation on inclined mhd flow of williamson fluid through a permeable wall with chemical reaction via dtm. Math Model Eng Probl 2020;7(1):1–9. http://dx.doi.org/10.18280/mmep.070101.

[10] Akinshilo AT. Steady flow and heat transfer analysis of third grade fluid with porous medium and heat generation. Eng Sci Technol Int J 2017;20(6):1602–9. http://dx.doi.org/10.1016/j.jestch.2017.11.012.

[11] Akinshilo AT, Mabood F, Badruddin IA. Hydrothermal evaluation of tangent hyperbolic fluid transport and entropy generation through parallel plates. Waves Random Complex Media 2022;1–17. http://dx.doi.org/10.1080/17455030.2022.2105420.

[12] Mabood F, Khan WA, Ismail AIM. Approximate analytical solution of stagnation point flow and heat transfer over an exponential stretching sheet with convective boundary condition. Heat Transf—Asian Res 2015;44(4):293–304. http://dx.doi.org/10.1002/htj.21122.

[13] Mao K. A numerical method for polymer composite gear flash temperature prediction. Wear 2007;262:1321–9. http://dx.doi.org/10.1016/j.wear.2007.01.008.

[14] Raghuraman NP. A calculation procedure to account for tolerances, transient temperature and humidity in the load distribution analysis of plastic and metal gears (Master's thesis), Graduate School of The Ohio State University, The Ohio State University; 2013.

[15] Černe B, Duhovnik J, Tavčar J. Semi-analytical flash temperature model for thermoplastic polymer spur gears with consideration of linear thermo-mechanical material characteristics. J Comput Des Eng 2019;6(4):617–28. http://dx.doi.org/10.1016/j.jcde.2019.03.001.

[16] Handschuh RF. Thermal behavior of spiral bevel gears. Tech. rep., Lewis Research Center; 1995.

[17] Patir N, Cheng HS. Prediction of the bulk temperature in spur gears based on finite element temperatureanalysis. ASLE Trans 1979;22:25–36. http://dx.doi.org/10.1080/05698197908982899.

[18] Winter AD, Blok H. Fling-off cooling of gear teeth. ASME pap, 1972, p. 60–70.

[19] van Heijningen GJJ, Blok H. Continuous as against intermittent fling-off cooling of gear teeth. J Lubr Technol 1974;96(4):529–38. http://dx.doi.org/10.1115/1.3452476.

[20] Handschuh RF, Kicher TP. A method for thermal analysis of spiral bevel gears. J Mech Des 1996;118:580–5.

[21] Holman JP. Heat transfer. 10th ed.. New York: McGraw-Hill; 2010.

[22] Hartnett J, Deland E. The influence of prandtl number on the heat transfer from rotating nonisothermal disks and cones. J Heat Transfer 1961;83:95–6. http://dx.doi.org/10.1115/1.3680479.

[23] Long H, Lord AA, Gethin DT, Roylance BJ. Operating temperatures of oil-lubricated medium-speed gears: numerical models and experimental results. Proc Instn Mech Engrs 2003;217. http://dx.doi.org/10.1243/095441003765208745.

[24] Popiel CO, Bogusławski L. Local heat-transfer coefficients on the rotating disk in still air. Int J Heat Mass Transfer 1975;18:167–70. http://dx.doi.org/10.1016/0017-9310(75)90020-4.

[25] Dorfman L. Hydrodynamic resistance and the heat loss of rotating solids. Oliver & Boyd; 1963.

[26] Taburdagitan M, Akkok M. Determination of surface temperature rise with thermo-elastic analysis of spur gears. Wear 2006;261:656–65. http://dx.doi.org/10.1016/j.wear.2006.01.019.

[27] Shi Y, Yao YP, Fei JY. Analysis of bulk temperature field and flash temperature for locomotive traction gear. Appl Therm Eng 2016;99:528–36. http://dx.doi.org/10.1016/j.applthermaleng.2016.01.093.

[28] Luo B, Li W. Influence factors on bulk temperature field of gear. Proc Inst Mech Eng J 2017;231:953–64. http://dx.doi.org/10.1177/1350650116684275.

[29] Li W, Tian J. Unsteady-state temperature field and sensitivity analysis of gear transmission. Tribol Int 2017;116:229–43. http://dx.doi.org/10.1016/j.triboint.2017.07.019.

[30] Li W, Zhai P, Ding L. Analysis of thermal characteristic of spur/helical gear transmission. J Therm Sci Eng Appl 2019;11. http://dx.doi.org/10.1115/1.4041597.

[31] Li W, Zhai P, Tian J, Luo B. Thermal analysis of helical gear transmission system considering machining and installation error. Int J Mech Sci 2018;149:1–17. http://dx.doi.org/10.1016/j.ijmecsci.2018.09.036.

[32] Doll N. Modeling thermomechanical behavior of polymer gears (Master's thesis), Department of Mechanical Engineering, University of Wisconsin-Madison; 2015.

[33] Doll N, Verdesca A, Bastos E, Osswald T, Kleiss R. Methodology for quasi-viscoelastic simulation of polymer gears made from PEEK using Ansys. In: Proceedings of the ANTEC. 2015.

[34] Latour B, Bouvier P, Harmand S. Convective heat transfer on a rotating disk with transverse air crossflow. J Heat Transfer 2011;133. http://dx.doi.org/10.1115/1.4002603.

[35] Özerdem B. Measurement of convective heat transfer coefficient for a horizontal cylinder rotating in quiescent air. Int Commun Heat Mass Transfer 2000;27(3):389–95. http://dx.doi.org/10.1016/S0735-1933(00)00119-6.

[36] Fernandes C, Rocha DM, Martins RC, Magalhães L, Seabra JH. Finite element method model to predict bulk and flash temperatures on polymer gears. Tribol Int 2018;120:255–68. http://dx.doi.org/10.1016/j.triboint.2017.12.027.
[37] Roda-Casanova V, Sanchez-Marin F. A 2D finite element based approach to predict the temperature field in polymer spur gear transmissions. Mech Mach Theory 2019;133:195–210. http://dx.doi.org/10.1016/j.mechmachtheory.2018.11.019.
[38] Roda-Casanova V, Gonzalez-Perez I. Investigation of the effect of contact pattern design on the mechanical and thermal behaviors of plastic-steel helical gear drives. Mech Mach Theory 2021;164. http://dx.doi.org/10.1016/j.mechmachtheory.2021.104401.
[39] Černe B, Petkovšek M, Duhovnik J, Tavčar J. Thermo-mechanical modeling of polymer spur gears with experimental validation using high-speed infrared thermography. Mech Mach Theory 2020;146. http://dx.doi.org/10.1016/j.mechmachtheory.2019.103734.
[40] Wang Y, Niu W, Chen Y, Song G, Tang W. Convection heat transfer and temperature analysis of oil jet lubricated spur gears. Ind Lubr Tribol 2016;68:624–31. http://dx.doi.org/10.1108/ILT-10-2015-0145.
[41] Concli F, Gorla C. A CFD analysis of the oil squeezing power losses of a gear pair. Int J Comput Methods Exp Meas 2014;2:157–67. http://dx.doi.org/10.2495/CMEM-V2-N2-157-167.
[42] Mastrone MN, Concli F. Cfd simulations of gearboxes: implementation of a mesh clustering algorithm for efficient simulations of complex system's architectures. Int J Mech Mater Eng 2021;16. http://dx.doi.org/10.1186/s40712-021-00134-6.
[43] Mastrone M, Hartono E, Chernoray V, Concli F. Oil distribution and churning losses of gearboxes: Experimental and numerical analysis. Tribol Int 2020;151. http://dx.doi.org/10.1016/j.triboint.2020.106496.
[44] Lu F, Wang M, Pan W, Bao H, Ge W. CFD-Based investigation of lubrication and temperature characteristics of an intermediate gearbox with splash lubrication. Appl Sci 2021;11(1). http://dx.doi.org/10.3390/app11010352.
[45] Liu H, Link F, Lohner T, Stahl K. Computational fluid dynamics simulation of geared transmissions with injection lubrication. Proc Inst Mech Eng C 2019;233:7412–22. http://dx.doi.org/10.1177/0954406219865920.
[46] Renjith S, Srinivasa VK, U. Venkateshaiah, thermal performance prediction of jet lubricated transmission system using computational methods. SAE technical papers 2017-october, 2017, http://dx.doi.org/10.4271/2017-01-2437.
[47] Deshpande S, Joshi H, Madhavan J, Mason P, Wink C. Two-way coupled cfd approach for predicting gear temperature of oil jet lubricated transmissions. SAE Int J Commer Veh 2018;11:163–70. http://dx.doi.org/10.4271/02-11-03-0013.
[48] Kara E, Nas ÖF, Yıldırım N. Cfd simulation of turbulent flow around a shrouded spur gear for predicting load-independent windage power losses. In: Burnete N, Varga BO, editors. Proceedings of the 4th international congress of automotive and transport engineering (AMMA 2018). Cham: Springer International Publishing; 2019, p. 25–31.
[49] Ouyang T, Mo X, Lu Y, Wang J. Cfd-vibration coupled model for predicting cavitation in gear transmissions. Int J Mech Sci 2022;225. http://dx.doi.org/10.1016/j.ijmecsci.2022.107377.
[50] Çengel Y. Heat transfer: a practical approach. McGraw-Hill; 2003.
[51] Guelfi A, Bestion D, Boucker M, Boudier P, Fillion P, Grandotto M, Hérard J-M, Hervieu E, Péturaud P. Neptune: A new software platform for advanced nuclear thermal hydraulics. Nucl Sci Eng 2007;156(3):281–324. http://dx.doi.org/10.13182/NSE05-98.
[52] Sanderse B, Van Der Pijl S, Koren B. Review of computational fluid dynamics for wind turbine wake aerodynamics. Wind Energy 2011;14(7):799–819. http://dx.doi.org/10.1002/we.458.
[53] Samstag R, Ducoste J, Griborio A, Nopens I, Batstone D, Wicks J, Saunders S, Wicklein E, Kenny G, Laurent J. CFD for wastewater treatment: An overview. Water Sci Technol 2016;74(3):549–63. http://dx.doi.org/10.2166/wst.2016.249.
[54] Karpinska AM, Bridgeman J. CFD-aided modelling of activated sludge systems - a critical review. Water Res 2016;88:861–79. http://dx.doi.org/10.1016/j.watres.2015.11.008.
[55] Iserte S, Macías A, Martínez-Cuenca R, Chiva S, Paredes R, Quintana-Ortí ES. Accelerating urban scale simulations leveraging local spatial 3D structure. J Comput Sci 2022;62:101741. http://dx.doi.org/10.1016/j.jocs.2022.101741.
[56] Wen T, Lu L, Luo Y. Review on the fundamentals and investigations of falling film dehumidification/absorption refrigeration based on CFD technology. Int J Heat Mass Transfer 2021;171:121042. http://dx.doi.org/10.1016/j.ijheatmasstransfer.2021.121042.
[57] Barbera-Domingo M, Martinez-Cuenca R, Roda-Casanova V, Sanchez-Marin F, Chiva S. Numerical investigation on the convective heat transfer coefficient of polymer spur and helical gears. In: Book of abstracts, FTPO international conference: plastic gears. 2021.
[58] Menter FR. Two-equation eddy-viscosity turbulence models for engineering applications. 1994, http://dx.doi.org/10.2514/3.12149.
[59] Baliga B, Patankar S. A new finite-element formulation for convection–diffusion problems. Numer Heat Transfer 1980;3:393–409. http://dx.doi.org/10.1080/01495728008961767.
[60] Kim J-H, Lee H-C, Kim J-H, Choi Y-S, Yoon J-Y, Yoo I, Choi W-C. Improvement of hydrodynamic performance of a multiphase pump using design of experiment techniques. J Fluids Eng 2015;137:081301. http://dx.doi.org/10.1115/1.4029890, (15pp).
[61] Jeong W, Seong J. Comparison of effects on technical variances of computational fluid dynamics (cfd) software based on finite element and finite volume methods. Int J Mech Sci 2014;78:19–26. http://dx.doi.org/10.1016/j.ijmecsci.2013.10.017.
[62] Franke J, Baklanov A. Best practice guideline for the CFD simulation of flows in the urban environment: COST action 732 quality assurance and improvement of microscale meteorological models. 2007.
[63] Tanaka M, Ohno S, Ohshima H. Development of V2UP (V & V plus uncertainty quantification and prediction) procedure for high cycle thermal fatigue in fast reactor—framework for V & V and numerical prediction. Nucl Eng Des 2016;299:174–83. http://dx.doi.org/10.1016/j.nucengdes.2015.07.010, cFD4NRS-5.
[64] Arnau R, Climent J, Martinez-Cuenca R, Rodriguez J, Chiva S. Evaluation of hydraulic mixing performance in a full-scale anaerobic digester with an external liquid recirculation system using CFD and experimental validation. Chem Eng Sci 2022;251:117392. http://dx.doi.org/10.1016/j.ces.2021.117392.
[65] Peskin C. Flow patterns around heart valves: a digital computer method for solving the equations of motion. IRE Trans Med Electron 1973;BME-20(4):316–7.
[66] Mastrone M, Concli F. Cfd simulation of grease lubrication: Analysis of the power losses and lubricant flows inside a back-to-back test rig gearbox. J Non-Newton Fluid Mech 2021;297. http://dx.doi.org/10.1016/j.jnnfm.2021.104652.
[67] Burberi E, Fondelli T, Andreini A, Facchini B, Cipolla L. Cfd simulations of a meshing gear pair. ASME; 2016, http://dx.doi.org/10.1115/GT2016-57454.
[68] Martínez-Cuenca R, Mondragón R, Hernández L, Segarra C, Jarque J, Hibiki T, Juliá J. Forced-convective heat-transfer coefficient and pressure drop of water-based nanofluids in a horizontal pipe. Appl Therm Eng 2016;98:841–9. http://dx.doi.org/10.1016/j.applthermaleng.2015.11.050.
[69] Milly P, Toledo R, Kerr W, Armstead D. Hydrodynamic cavitation: characterization of a novel design with energy considerations for the inactivation of saccharomyces cerevisiae in apple juice. J Food Sci 2008;73:298–303. http://dx.doi.org/10.1111/j.1750-3841.2008.00827.x.
[70] Takanashi S, Shoji A. On the equilibrium temperature in the teeth of operating plastic gears. Bull Yamagata Univ 1984;18:11–24.
[71] Cardone G, Astarita T, Carlomagno G. Heat transfer measurements on a rotating disk. Int J Rotating Mach 1997;3(1):1–9. http://dx.doi.org/10.1155/S1023621X97000018.
[72] Černe B, Petkovšek M. High-speed camera-based optical measurement methods for in-mesh tooth deflection analysis of thermoplastic spur gears. Mater Des 2022;223:111184. http://dx.doi.org/10.1016/J.MATDES.2022.111184.
[73] Letzelter E, Guingand M, de Vaujany J-P, Schlosser P. A new experimental approach for measuring thermal behaviour in the case of nylon 6/6 cylindrical gears. Polym Test 2010;29:1041–51. http://dx.doi.org/10.1016/j.polymertesting.2010.09.002.
[74] Raush G, Gamez-Montero P, Castilla R, Codina E. Experimental study on the impulsion port of a trochoidal wheeled pump. Flow Meas Instrum 2017;55:13–22. http://dx.doi.org/10.1016/j.flowmeasinst.2016.10.014.
[75] Knudsen J, Katz D. Fluid dynamics and heat transfer. Chemical engineering series, McGraw-Hill; 1958.
[76] Millsaps K, Pohlhausen K. Heat transfer by laminar flow from a rotating plate. J Aeronaut Sci 1951;18(5):354–5. http://dx.doi.org/10.2514/8.1955.